8th International Symposium on Magnetic Bearing
August 26-28, 2002, Mito, Japan

A NOVEL SINGLE DEGREE-OF-FREEDOM ACTIVE VIBRATION ISOLATION SYSTEM

Tsuyoshi Sato
TOSHIBA CORPORATION, Yokohama, Kanagawa-Pref., 235-0017 Japan
tsuyoshi2.sato@toshiba.co.jp

David L. Trumper
Dept. of Mechanical Eng., Massachusetts Institute of Technology, Cambridge, MA,02139 USA
trumper@mit.edu

ABSTRACT

A prototype of a single degree-of-freedom active vibration isolation system is developed with a novel actuator design and control algorithm. In our actuator design, two variable reluctance actuators face each other with two thin sheets of elastomeric material placed between each actuator and the suspended mass. Using the tunable negative spring of the variable reluctance actuators, we can realize the required soft spring even with the thin elastomeric material sheets and can dramatically downsize the actuator unit. Hybrid position and velocity control system is developed to enable both good vibration isolation performance and platform re-leveling. We demonstrate our system's disturbance rejection performance against floor vibration and on-board generated disturbance force and show our actuator-design concept and control algorithm have significant promise.

INTRODUCTION

Active vibration isolation technology is receiving increasing attention as the means to insulate precision machines from floor vibration and at the same time reject on-board-generated disturbance forces. This is happening because conventional passive mounts such as elastomers and pneumatic isolators have a fundamental trade-off between rejecting these two classes of disturbance [1].

Many present-day active isolation systems use a parallel architecture of soft passive springs to support the static load and electromechanical actuators to provide the active force control. However there is a problem with this configuration in terms of the difference of traveling distance between the passive mount and the actuator. According to the Bolt Beranek & Newman Inc. (BBN) criteria, which are historically the first set of criteria to characterize vibration environments in micro-electronics facilities and are widely used in the design of those facilities, the floor motion never exceeds 8 μm for VC-A class machines such as optical microscopes to 400X, microbalances, optical balances, proximity and projection aligners [2]. Our application may be used in environment with smaller floor vibration than VC-A's condition, thus tens of microns should be enough as the required traveling distance for active isolation actuators. Meanwhile the traveling distance of the passive mount is generally from hundreds of microns to tens of millimeters and it is thus much larger than that of the actuator. This is because the dimensions of the passive mount are determined by the natural frequency and damping requirements of the system. In general, the lower the natural frequency, the better the isolation system performance. In order to realize the required soft springs, the passive springs typically require a large packaging volume.

Another issue relates to the system actuators. Typically, Lorenz-type actuators (voice coils or linear motors) are used to drive the active control forces.

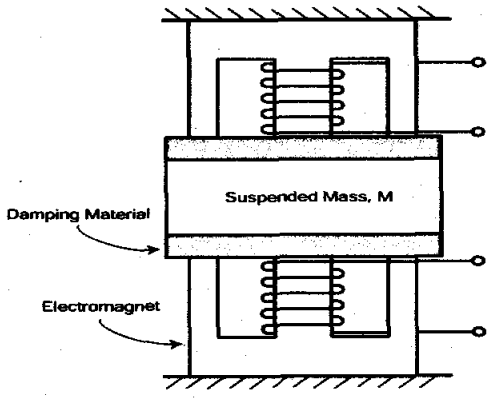

FIGURE 1: A novel actuator unit for a single dof active vibration isolation system.

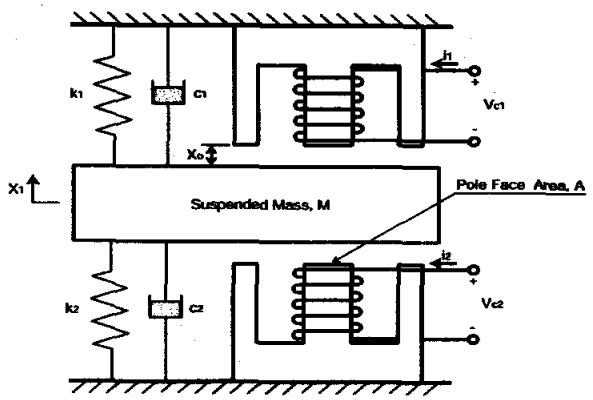

FIGURE 2: A schematic representation of the experimental system. x_1 is the displacement from the center of the two electromagnets, at a distance x_o from each pole face. Damping coefficient, spring constant, control current and input voltage for the upper actuator are represented as c_1, k_1, i_1 and V_{c1}, respectively. Those values for the lower actuator are designated as c_2, k_2, i_2 and V_{c2} in the same way.

However, such actuators have low force per power as compared with variable reluctance actuators. Thus we have investigated the possibility of using variable reluctance actuators to drive our isolation system.

The downside of such actuators is their nonlinear force/current/air-gap relationship, which makes it hard to achieve high isolation performance. The actuators also have a negative equivalent spring constant which makes the open-loop system unstable. To address this, we have paired the variable reluctance actuators with a thin sheet of elastomeric material as shown in FIGURE 1. If we can realize sufficiently low natural frequency even with thin elastomers, and with good damping, we could dramatically downsize the isolation system. This point is our motivation to develop a novel compact actuator for active vibration isolation; this compact actuator could gain wider application in many industries such as electronics, semiconductors and optics.

ACTUATOR DESIGN AND EXPERIMENTAL HARDWARE

Our actuator design is schematically represented in FIGURE 2. The basic idea of our design is that relative high positive spring constant of the thin damping material, k_d, the sum of k_1 and k_2, can be counterbalanced with the tunable negative spring constant of the variable reluctance actuators, k_x. The derivation of k_x will be stated in the following section. The total spring constant, k_l is derived as follows,

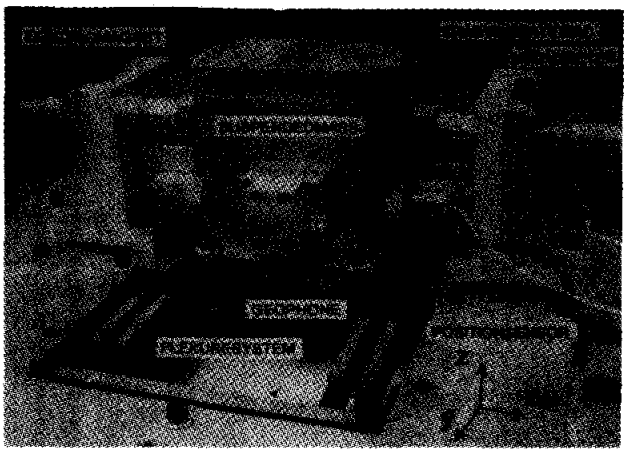

FIGURE 3: A single dof platform of the active vibration isolation. The suspended mass weighs 20 kg and the center of gravity is 50.8 mm high from the upper surface of the low carbon steel plate. All sensors and actuators are placed at this height. Without damping material, the estimated 1st-mode natural frequency is 3.5 Hz according to the planar analysis detailed in [3]. The experimental result of the 1st-mode is 3.0 Hz and well matched to the calculated value.

$$k_l = k_d - k_x \tag{1}$$

and is thereby set to small positive value which leads to the required low natural frequency of the isolation system even with the thin damping material sheets.

Based on the same principle, we have built the prototype of the single dof active vibration isolation system shown in FIGURE 3. The double compound rectilinear spring is made from 1 inch-thick low carbon steel plate to realize x-direction motion of the suspended mass and to constrain other five uncontrolled dof. Note that the setup of the prototype is horizontal even though the setup in FIGURE 2 is vertical.

Commonly used Sorbothane with 50 durometer is used as damping material for our system. Each 1.5 mm-thick Sorbothane sized to 18 $mm \times 18$ mm is placed between the suspended mass and a fixture with a tapered hole. This fixture forms kinematic coupling with a steel ball glued to the tip of a micrometer. The damping material sheets are preloaded by the micrometers and are compressed by about 20 %. For convenience of experiments, the gap of the electromagnet and thickness of the damping material sheet should be changed independently, thus we separate the electromagnet and the damping material sheet in this prototype.

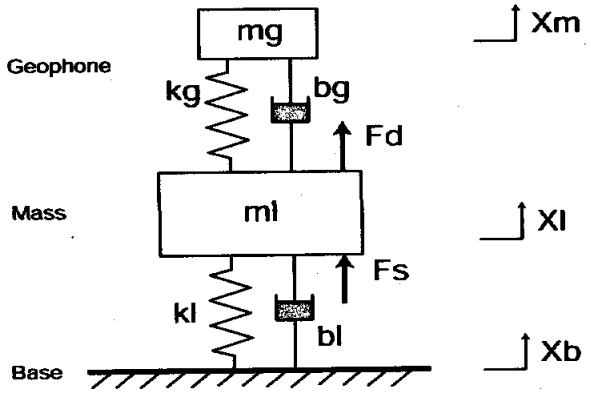

FIGURE 4: System mechanical model. Inside the outer housing of the geophone, a moving mass $m_g = 11.2g$ is supported by a flexure with stiffness $k_g = 44.2N/m$ and damping $b_g = 0.445Ns/m$. The output voltage of the geophone, $V_{out} = B_g l_g(\dot{X}_m - \dot{X}_l)$. The product value of B_g and l_g is specified by the manufacturer as $B_g l_g = 27.5Vs/m$.

The position of the suspended mass is controlled via two electromagnetic actuators. Each electromagnet consists of a 12.7 mm-thick stack of E-core laminations. The center leg of the core is surrounded by 230 turns of ♯22 magnetic wire on a nylon bobbin. The cross section area of the center pole is 161 mm^2 and the area of each of the two outer poles is half of this value. Each air gap between the electromagnet and a target I-shape lamination, mounted on the both side of the mass, is 110 μm. The laminations used in our magnetic suspensions are made from 50 % Ni, 50 % Fe material.

The position and the velocity of the suspended mass are sensed by a pair of eddy current-type position sensors made by Kaman and a geophone, model GS30CT 10-395 HORZ made by OYO Geospace, respectively.

CONTROL ALGORITHM

Considering the basic mechanical structure of the isolation system shown in FIGURE 2 and the geophone, a two degree-of-freedom structural system model is constructed as observed in FIGURE 4. Here X_m, X_l and X_b are the displacements of the proof mass, the outer housing of the geophone and the floor with respect to inertial space, respectively. F_s is the force provided by electromagnets and F_d is the disturbance force applied to the mass. In order to facilitate the design of the controller for vibration isolation, we use the model with the shifted natural frequency from 60 Hz, original natural frequency of the passive mount, to 25 Hz and thus we set the total spring constant $k_l = 5.1 \times 10^5 N/m$ in our model.

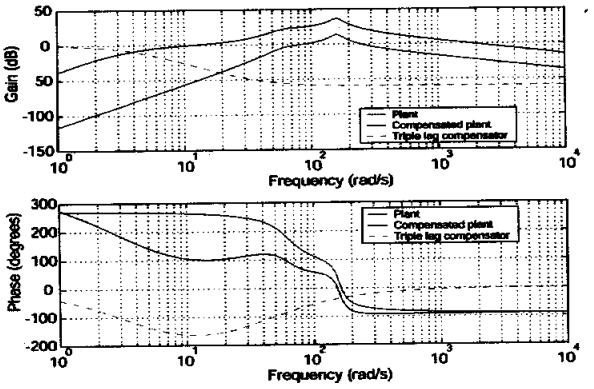

FIGURE 5: Transfer functions used in the controller design process.

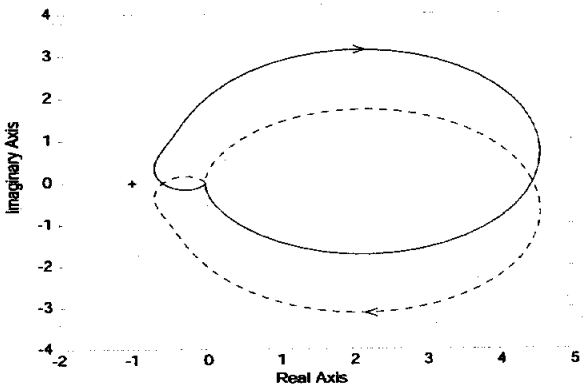

FIGURE 6: Nyquist plot for the system with a unity gain compensator.

The total damping coefficient, the sum of c_1 and c_2, $b_l = 667Ns/m$ is obtained by the experimental transient performance of the passive mount.

Then we develop a state-space-based model for our active isolation system according to the modeling process, detailed in [4], for a single dof active vibration isolation system using geophone as velocity sensor.

Controller design for the active isolation

The calculated plant transfer function from F_s to V_{out} is shown in FIGURE 5. This plot clearly shows that the plant is AC-coupled with three zeros at the origin, and two pairs of complex poles.

The active control bandwidth is between the two crossover points. In order to get good isolation performance, we need to make the active bandwidth wide and the loop gain as large as possible in the bandwidth. Since the upper unity-gain frequency is limited by structural resonances and the lower one is limited by noise in the inertial sensor [5], we set the active control bandwidth at between 13 rad/s (2 Hz) and 1885 rad/s (300 Hz).

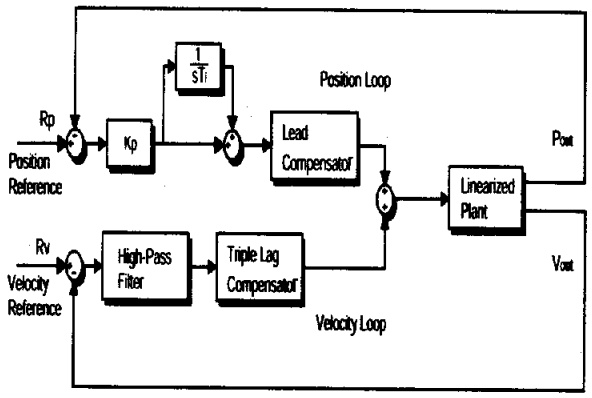

FIGURE 7: Hybrid (position/velocity) control diagram. PI controller with proportional gain $K_p = 0.4$ and integral time $T_i = 0.008$ *sec* is used as the compensator for the position loop. All compensator is implemented to dSPACE DS1103 board with a selected sample rate of 10 kHz.

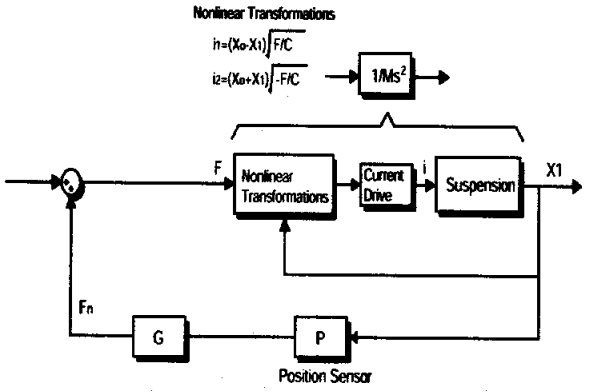

FIGURE 8: Linearized plant. Linear negative spring is produced by feedback linearization and positive position feedback.

The Nyquist plot shown in FIGURE 6 addresses how to compensate the system. According to the FIGURE 6, the system may have two encirclements of -1 and thus two unstable closed-loop poles with the increase of the open loop gain. In order to stabilize the loop, negative phase should be added to the loop at the low frequency unity-gain crossover. Our target phase margin is 70° at 13 rad/s and thus we need to add $-160°$ phase shift to move the loop phase down from about $+270°$ to $+110°$. We use a triple lag compensator of the form $K_c(\frac{\tau_1 s+1}{\alpha\tau_1 s+1})^3$, with $\alpha = 10$ and $\tau_1 = 0.026$ sec. The controller gain $K_c = 1.3 \times 10^4$ is chosen to set the loop crossover at 13 rad/sec.

Since this triple lag compensator gives a large DC gain, any offset in the measurement chain causes large force offset. In order to prevent any undesirable DC control action, we put the high-pass filter of the form $\frac{\tau_2 s}{\tau_2 s+1}$, with $\tau_2 = 1$ sec in the velocity loop.

Calculated loop transmission of the compensated plant in FIGURE 5 shows that the specifications of the controller are well satisfied in terms of the phase margin and the active bandwidth.

Hybrid control and linear negative spring

The suspended mass could be moved by the disturbance vibration with lower frequency than the active control bandwidth shown in FIGURE 5. We thereby need position control to eliminate the mass drift caused by the low frequency disturbance and build the hybrid position and velocity control system with the parallel configuration, as shown in FIGURE 7.

When the suspended mass separates from the center to either side, negative spring constant, k_x, exponentially increases and k_l goes to be negative according to (1). This means that the system turns to be unstable and the suspended mass sticks to either actuator's pole. Thus we also need to produce a linear negative spring constant to mitigate the exponential increase of negative spring, k_x. To do so, we linearize the system by feedback linearization and then the position signal is positively fedback. We can get the linear negative spring according to the following process.

As stated earlier, variable reluctance actuators have nonlinear relationship between the generated force, air gap and control current as follows,

$$F_1 = C\frac{i_1^2}{(x_o - x_1)^2} \tag{2}$$

$$F_2 = -C\frac{i_2^2}{(x_o + x_1)^2} \tag{3}$$

$$C = \frac{\mu_o N^2 A}{4} \tag{4}$$

where F_1 and F_2 are the electromagnet force of each actuator, C is the actuator constant, μ_o is the permeability of free space and is given as $4\pi\times10^{-7} H/m$, N is the number of turns of coil and A is the pole face area. Note that the finite permeability of the core is modeled simply by using the equivalent air gap, 20 μm, and this air gap is included into x_o.

According to these equations, we can get nonlinear transformations as follows,

$$\begin{aligned} i_1 &= (x_o - x_1)\sqrt{\frac{F}{C}} \quad , \quad i_2 = 0 \quad (F > 0) \\ i_2 &= (x_o + x_1)\sqrt{\frac{-F}{C}} \quad , \quad i_1 = 0 \quad (F < 0) \end{aligned} \tag{5}$$

where F represents the desired force. The system can be linearized if the two coil currents vary

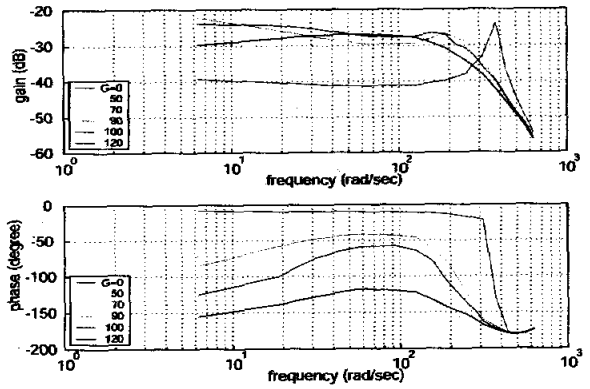

FIGURE 9: Measured plant transfer functions from desired force F to the output of the position sensor P_{out}. In this experiment, the system runs only with the position loop. $G = 0$ indicates the original natural frequency. Note that the position controller gain K_p is equal to 3 for every value of G, except for $G = 120$ where K_p is set to 15 to avoid instability.

in accordance with the equations above. Note that, as viewed in FIGURE 8, the relationship between F and x_1 is equal to a double integrator multiplied by $1/M$, independent of operating point. When we close a position loop with the positive feedback, the desired negative spring force F_n is expressed as below and we can get the linear negative spring constant, k_{xl}, as follows.

$$F_n = k_{xl} x_1 \tag{6}$$

$$k_{xl} = GP \tag{7}$$

where G is the feedback gain of the position loop to adjust the negative spring and $P = 3.3 \times 10^4$ is the gain of the position sensor.

The application of feedback linearization to the dual magnetic suspension system like our system is well described in [6].

FIGURE 9 indicates that we successfully change the natural frequency by tuning negative spring. It also shows that an interesting phase drop occurs with the increasing negative spring value. Our estimated reason for this phenomenon is the following. As well known, the damping material has the dynamic modulus [7] and thus its stiffness decreases with the decreasing frequency. Since the negative spring of the electromagnets is constant, the total stiffness would become negative somewhere in low frequencies and the phase of the system would approach $-180°$. The larger negative spring makes this phase drop faster to $-180°$.

In the hybrid system, this phase drop significantly affects the stability of the system because it directly reduces the phase margin of the position loop. In

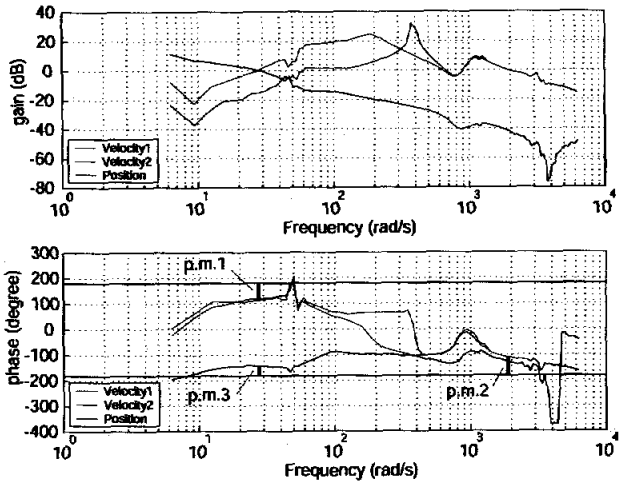

FIGURE 10: Open-loop transfer functions of the hybrid system measured by digital signal analysis program [8] under MATLAB and SIMULINK environment. The loop transfer function of the velocity loop with the shifted natural frequency, 25 Hz, and that with original natural frequency, 60 Hz, are labeled as Velocity 1 and Velocity 2, respectively. The loop transfer function of the position loop with the shifted natural frequency is labeled as Position.

order to compensate for this phase drop, a lead compensator of the form $\frac{\alpha\tau_3 s+1}{\tau_3 s+1}$, with $\alpha = 15$ and $\tau_3 = 0.022$ sec, is placed in the position loop. This lead compensator gives us $+60°$ phase lead at 12 rad/s.

Measured open-loop transfer functions of the hybrid system is shown in FIGURE 10. The active bandwidth of Velocity 1 is between 28 rad/s (4.5 Hz) and 1885 rad/s (300 Hz) and the measured phase margins, $p.m.1 = 61°$ at 28 rad/s and $p.m.2 = 70°$ at 1885 rad/s for velocity loop and $p.m.3 = 37°$ at 28 rad/s for position loop, shows that this hybrid system is stable.

EXPERIMENTAL RESULT

In order to ascertain the performance of the active vibration isolation system, we perform two sets of experiments, a seismic transmissibility test and a transient performance (settling time) test. The result of the transmissibility test is plotted in FIGURE 11. The passive transmissibility (dashed line) clearly shows the resonant peak due to the passive mount. The active transmissibility (solid line) with the shifted natural frequency, 25 Hz, indicates a clear attenuation in the active control region and the maximum attenuation is about 35 dB.

The result of the transient performance test is shown in FIGURE 12 where the acceleration of the passive mount, active mount and impact hammer

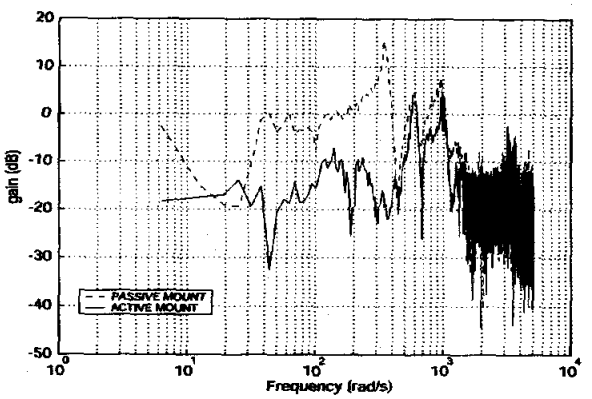

FIGURE 11: Measured transmissibility. Floor vibrations in the horizontal direction are measured using a seismic accelerometer attached to the surface plate on which the prototype is placed. The horizontal vibrations of the suspended mass are similarly measured by a accelerometer attached to the suspended mass. The transfer function between these two accelerations is calculated by the HP 35665A signal analyzer. The surface plate is excited by PCB 086C20 impact hammer, which provides uniform excitation by about 1257 rad/s (200 Hz). The average number of this test is 20 times.

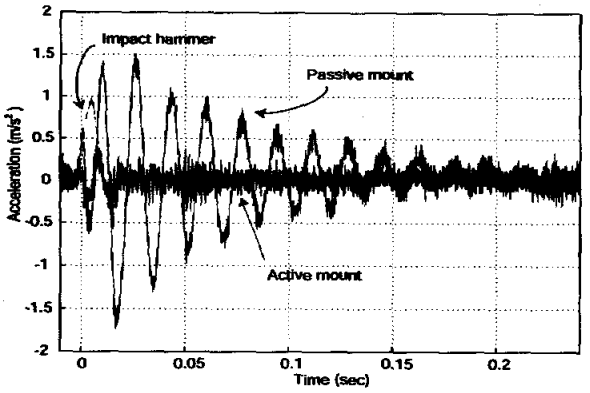

FIGURE 12: Isolation performance in time domain after impact. The acceleration of the suspended mass is measured by the same setup in the seismic transmissibility test. The force disturbance is provided by hitting the suspended mass using the impact hammer.

are plotted. When the active system is turned off, the rocking of the acceleration plot of the suspended mass is consistent with its natural frequency due to the passive mount. When the active system is turned on, the rocking at the natural frequency is found to be arrested just after the moment when the acceleration provided by the impact hammer turns to be negative.

CONCLUSION AND FURTHER WORK

Our novel idea to produce soft spring using thin elastomeric material sheets and the variable reluctance actuators has been introduced. We have built the prototype of the single dof active vibration isolation system and have performed two sets of experiments showing significant benefits of the active vibration isolation. Since our system has possibility to make the isolation system much smaller than present-day isolation systems, it is a promising candidate as means of disturbance rejection for next-generation precision machines.

The next step is to add bias flux using permanent magnets to support large static load without excessive generation of heat caused by drive currents in case of a vertical setup.

ACKNOWLEDGMENT

The first author wishes to acknowledge members of Precision Motion Control Laboratory in MIT for their helpful discussions about flexure design and a hybrid control issue. This work is supported by Corporate Manufacturing Engineering Center of TOSHIBA CORPORATION.

References

1. Subrahmanyan,P.K., Ph.D. dissertation, Dept. Mech. Eng. MIT, Cambridge, MA, Sept. 1999.
2. Gordon,C.G., Generic criteria for vibration-sensitive equipment, SPIE Proc., volume 1619, SanJose CA, 4-6 Nov. 1991.
3. Smith,S.T., Flexure, Gordon and Breach Science Publishers, 1st edition, 2000.
4. Trumper,D.L. and Sato,T., A vibration isolation platform, Mechatronics 2000, Atlanta GA, 6-8 Sept. 2000.
5. Nelson,P.G., An active vibration isolation system for inertial reference and precision measurement, Rev. Sci. Instrum., volume 62, Sept. 1991
6. Trumper,D.L., Olson,S.M. and Subrahmanyan,P.K., Linearizing Control of Magnetic Suspension Systems, IEEE Trans. on Control Systems Technology, vol.5, no.4, July 1997.
7. Nashif,A.D., Jones,D.I.G. and Henderson,J.P., Vibration Damping, John Wiley & Sons, 1985.
8. Lillienkamp,K., Dynamic Signal Analyzer Implemented on dSPACE System, BS thesis, Dept. Mech. Eng. MIT, Cambridge, MA, Jan. 1999.